Mathematical and Computer Modelling 58 (2013) 204–218

Contents lists available at SciVerse ScienceDirect

Mathematical and Computer Modelling

journal homepage: www.elsevier.com/locate/mcm

A new logo watermarking based on redundant fractional wavelet transform

Gaurav Bhatnagar *, Q.M. Jonathan Wu

Department of Electrical and Computer Engineering, University of Windsor, Windsor, Ontario, ON, N9B 3P4, Canada

ARTICLE INFO

Article history:
Received 28 February 2011
Accepted 12 June 2012

Keywords:
Digital watermarking
Redundant fractional wavelet transform
Automatic thresholding
Toral automorphism
Singular value decomposition

ABSTRACT

In this paper, a new watermarking scheme based on redundant fractional wavelet transform is presented. First, the definition and implementation of redundant fractional wavelet transform is proposed followed by its use in watermark embedding. For embedding, the gray-scale logo watermark is used and is embedded in the middle singular values of the redundant fractional wavelet domain. In order to enhance the security, a binary watermark is also embedded in the host image in lossless manner based on automatic thresholding. Finally, a reliable extraction process is developed for the extraction of both the watermarks from the possibly distorted image. The feasibility and robustness of the proposed technique is carried out by the security and attack analysis on different images.

1. Introduction

Due to the explosive growth in the development of electronic commerce and online services, the protection of multimedia contents has become an imperative issue. To tackle this problem, a notice or watermark is embedded in the multimedia which could help in the proof of origin and distribution of the multimedia content. Watermarking refers to the process of adding a message called a watermark to the original multimedia. The addition is made in such a way that it must not cause serious degradation of the original digital media. Such a watermark can be used for several purposes including copyright protection, fingerprinting, broadcast monitoring, and data authentication.

In the past few years, a large variety of watermarking techniques have been proposed in the literature. These algorithms can be broadly classified in two categories according to the embedding domain: spatial and transform domain. Spatial domain methods [1–4] are less complex as no transform is used, but are not robust against attacks. Transform domain methods are more robust in comparison to spatial domain methods. This is due to the fact that when an image is inverse transformed, the watermark is distributed irregularly over the image, making the attacker difficult to read or modify. In spatial domain methods, the watermark is embedded by modifying pixel intensities whereas in the transform domain original digital media is first transformed in the frequency domain by the means of Fourier transform [5], cosine transform [6], fractional Fourier transform [7,8], wavelet transform [9–15], wavelet packet transform [16,17], etc. Then, the transform domain coefficients are altered to embed the watermark and finally inverse transform is applied to obtain the watermarked digital media.

Schyndel et al. [1] have proposed two methods in which the first one is based on bit plane manipulation of the LSB whereas the second method utilizes the linear addition of the watermark to the image data, which is more difficult to decode, offering inherent security. Lee and Tsai [2] have proposed a new method in which embedding is performed by considering a human vision model with distortion-minimizing capabilities. For this purpose, the authors have proposed two optimization techniques, namely block pattern coding and dynamic programming to minimize distortion. Martin et al. [3] have proposed

* Corresponding author.
E-mail addresses: goravb@uwindsor.com (G. Bhatnagar), jwu@uwindsor.ca (Q.M. Jonathan Wu).

0895-7177/$ – see front matter © 2013 Published by Elsevier Ltd
doi:10.1016/j.mcm.2012.06.002

an informed watermarking scheme based on interpolation techniques. This scheme takes advantage of interpolation to generate imperceptible marks in the spatial domain. Lee and Lin [4] have proposed the use of watermarks for image tamper detection and recovery. Cox et al. [5] have presented the most popular watermarking schemes based on the Spread Spectrum Communication. The watermark is embedded into the first k highest magnitude DFT/DCT coefficients of the image and the extraction is done by comparing the DFT/DCT coefficients of the watermarked and the original image. Barni et al. [6] have proposed a watermarking algorithm, which operates in the frequency domain and embeds a pseudo-random sequence of real numbers in a selected set of DCT coefficients. Djurovic et al. [7] have proposed a fractional Fourier transform based watermarking scheme for the multimedia copyright protection. After decomposing the image via FRFT, transformation coefficients are reordered in a non-increasing sequence and the watermark is embedded in the middle coefficients. Feng et al. [8] have proposed a blind watermarking algorithm in which multiple chirps are used as a watermark and embedded in the spatial domain directly but detected in the FRFT domain. Barni et al. [9] have proposed a method based on the characteristics of the human visual system operating in a wavelet domain. Based on the texture and the luminance content of all image sub-bands, a mask is accomplished pixel by pixel. Kundur and Hatzinakos [10] have proposed the use of a gray scale logo as watermark. They have addressed a multiresolution fusion based watermarking method for embedding gray scale logos into wavelet transformed images via a salience factor. Wang and Lin [11] and Zhang et al. [12] have proposed a new watermarking algorithm based on wavelet tree quantization. Rahman et al. [13] have proposed a new detector for the DWT-based additive image watermarking, wherein a PDF based on the Gauss–Hermite expansion is used because this PDF provides a better statistical match to the empirical PDF by utilizing an appropriate number of parameters estimated from higher-order moments of the image coefficients. Lin and Lin [14] have proposed a lossless copyright protection scheme based on cryptography and watermarking. The basic idea is to generate a secret key during the embedding process using local features extracted from the perceptually prominent components of the host image in the wavelet domain followed by the digital signature and time-stamping technologies. Chou and Liu [15] have tried to satisfy the two conflicting requirements viz. transparency and robustness simultaneously. They exploit the fact that one can embed high-strength watermark signals in the host signals that can accommodate the distortion due to watermark insertion as part of perceptual redundancy. With the same idea, the authors have embedded one watermark in most distortion-tolerable signals within three color channels of the host image without resulting in perceivable distortion. Vehel and Manoury [16] have proposed a method in a wavelet packet domain. Instead of using the whole basis the authors have determined the sub-sets of the basis using a secret key and the energy criterion. Bhatnagar and Raman [17] have proposed a robust reference watermarking scheme, which uses a meaningful gray-scale logo as watermark, based on wavelet packet transform and bidiagonal singular value decomposition for copyright protection and authenticity.

Recently, a new transform, singular value decomposition (SVD)-based [18,19] watermarking technique and its variants have been proposed [20–26]. These approaches work on the simple concept of finding the SVD of a cover image or the SVD of each block of the cover image, and then modifying the singular values to embed the watermark. Liu and Tan [18] have proposed an algorithm based on SVD. In this algorithm, the authors find the singular values of the host image and then modify it by adding the watermark. SVD transform is again applied on the resultant matrix to find the modified singular values. These singular values are combined with the known component to get the watermarked image. The inverse process is used for the extraction of the watermark. Chandra [19] have described a method for embedding singular values of the watermark into the singular values of the entire image. Recently, some researchers have presented hybrid watermarking schemes in which they have combined SVD with other existing transforms. The SVD based scheme withstands a variety of attacks but it is not resistant to geometric attacks like rotation, cropping etc. Hence, for improving the performance hybridization is needed. Ganic and Eskicioglu [20] have presented a hybrid-watermarking scheme based on DWT and SVD. After decomposing the cover image into four bands, SVD is applied on each band, and then the singular values of each band with the singular values of the visual watermark are modified. Sverdlov et al. [21] have used the same concept taking DCT and SVD. DCT coefficients are mapped into four quadrants via ZIG-ZAG scan and then the singular values of each quadrant are modified. Li et al. [22] have proposed the same hybrid DWT-SVD domain watermarking scheme by exploiting the properties of the human visual system. Bhatnagar and Raman [23] have proposed a self reference watermarking scheme based on wavelet transform, directive contrast and SVD. Further authors have proposed another technique in which they utilize the rotation of the time-frequency plane over an arbitrary angle property of fractional Fourier transform in SVD based watermarking [27]. Chang et al. [24] have proposed a new technique in which embedding is done in D and U components.

In this paper, a new logo watermarking technique is presented which exploits the characteristics of the redundant fractional wavelet transform. The core idea of the proposed technique is to extend the size of host image with the help of reversible extension transform (RET) followed by the gray-scale watermark embedding in the middle singular values of the extended image. Since the largest singular values are more important for the image quality, and the smallest singular values are more sensitive to the noise, middle singular values are selected to embed the watermark. After embedding, inverse extension transform is applied to get the watermarked image. After getting the watermarked image, a verification phase is created with the help of toral automorphism and automatic thresholding. For this purpose, the watermarked image is shuffled using toral automorphism followed by the automatic thresholding to get a binary image. Now a binary watermark is embedded in a lossless manner. At the extraction end, first the binary watermark is extracted followed by the similarity evaluation between original and extracted binary watermarks. If the similarity is greater than the prescribed threshold then the possibly attacked watermarked image is verified and the extraction of the gray scale watermark is done. In other words, the gray scale watermark extraction is done if and only if the watermarked image is verified. Another benefit of the proposed

technique is that at least one of the watermarks (either gray scale or binary or both) can be extracted which further enhances the security of the image. Apart from the watermarking technique, a new transform, namely the redundant fractional wavelet transform is also proposed in the present work. The redundant fractional wavelet transform is the realization of the redundant wavelet transform in the fractional Fourier domain. A lifting based implementation of the redundant fractional wavelet transform is proposed and used in the present work.

The rest of paper is organized as follows: The explanation of used terminologies i.e. toral automorphism, singular value decomposition and automatic thresholding are given in Section 2. In Section 3, the detailed description of the redundant fractional wavelet transform is given. The proposed watermark embedding and extraction processes are described in the Section 4. Section 5 presents experimental results using proposed watermarking technique and finally the concluding remarks are given in Section 6.

2. Mathematical preliminaries

In this section, we provide the main terminologies which are used in the proposed algorithm to achieve the desired goal. These terminologies are as follows:

2.1. Toral automorphism

The toral automorphism [28] is the mapping from torus to torus. In the 2D case, the torus, say $\mathbb{T}^2$, can be viewed as the square where two points $(x_1,\ y_1)$ and $(x_2,\ y_2)$ are identified by either $x_1 = x_2, y_1 = y_2$ or one of the two coordinates is 0 and the other is 1. The simplest example of a torus is quotient group $\mathbb{R}^2/\mathbb{Z}^2$, where $\mathbb{R}^2$ is a topological group with addition operation and $\mathbb{Z}^2$ is a discrete subgroup of it. More precisely, toral automorphism is given as $\mathbf{r}' = T(\mathbf{r}) = A\mathbf{r}(\text{mod } 1)$ i.e.

$$\begin{bmatrix} x' \\ y' \end{bmatrix} = T\left(\begin{bmatrix} x \\ y \end{bmatrix}\right) = A\begin{bmatrix} x \\ y \end{bmatrix} (\text{mod } 1) \tag{1}$$

where $A = \begin{bmatrix} a & b \\ c & d \end{bmatrix}$ with integers $a,\ b,\ c,\ d$ and $det(A) = 1$. This matrix A plays a vital role in the iterated dynamical system formed by T. Mathematically, the dynamical system based on toral automorphism is expressed as $\mathbf{r}(n+1) = A\mathbf{r}(n)(\text{mod } 1)$, i.e.

$$\begin{bmatrix} x(n+1) \\ y(n+1) \end{bmatrix} = A\begin{bmatrix} x(n) \\ y(n) \end{bmatrix} (\text{mod } 1) \tag{2}$$

where $n = 0, 1, 2, \ldots$. If $a = 1,\ b = 1,\ c = 1$ and $d = 2$ then toral automorphism is reduced to cat-map. Hence, cat-map is a special case of toral automorphism. It essentially, stretches the unit square by transformation and then folds it into a square by a unit modulo operation. Hence, toral automorphism is area preserving. Toral automorphism can be easily extended from unit square to a square of length N by stretching the square of length N via transformation and then folding it into a square by N modulo operation. The typical working rule of toral automorphism is depicted in Fig. 1. Hence, the generalized toral automorphism is expressed as $\mathbf{r}(n+1) = A\mathbf{r}(n)(\text{mod } N)$ i.e.

$$\begin{bmatrix} x(n+1) \\ y(n+1) \end{bmatrix} = A\begin{bmatrix} x(n) \\ y(n) \end{bmatrix} (\text{mod } N). \tag{3}$$

Toral automorphism is a special class of Anosov Diffeomorphisms which are extreme chaotic systems obeying local instability, ergodicity with mixing and decay of correlation and periodic. Due to periodicity, the original square will reappear after some large number of iterations.

2.2. Singular value decomposition

Singular value decomposition (SVD) is a linear algebraic scheme, which was developed for a variety of applications. This transform was introduced for square matrices by Beltrami [29] and Jordan [30] and was extended to rectangular matrices by Eckart and Young [31].

Suppose A is a $m \times n$ matrix whose entries come from the field $\mathbb{K}$, which is either the field of real numbers or the field of complex numbers. Then there exists a factorization of the form

$$A = USV^T \tag{4}$$

where U is an $m \times m$ unitary matrix over K, the matrix S is a $m \times n$ diagonal matrix with non-negative real numbers on the diagonal and V^T denotes the conjugate transpose of V, an $n \times n$ unitary matrix over K. Such a factorization is called a singular-value decomposition of A. A common convention is to order the diagonal entries $S_{i,j}$ in non-increasing fashion. In this case, the diagonal matrix S is uniquely determined by A (though the matrices U and V are not). The diagonal entries of S are known as the singular values of A. The detailed explanation of SVD is as follows.

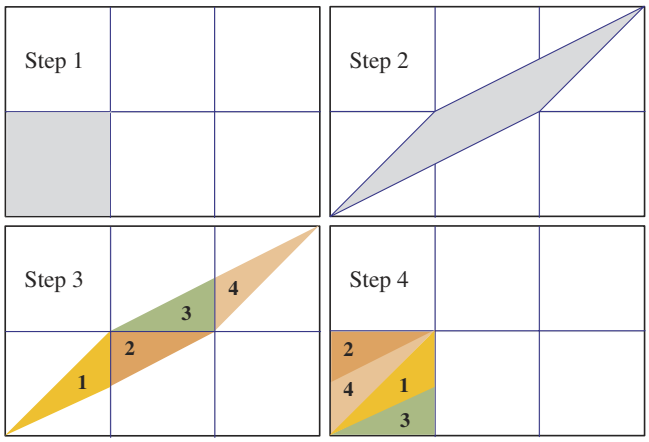

Fig. 1. A typical working rule for toral automorphism i.e. stretching (upper row of figure) and folding (lower row of figure).

(1) The columns of V form a set of orthonormal "input" or "analyzing" basis vector directions for A. (These are the eigenvectors of A^TA.)
(2) The columns of U form a set of orthonormal "output" or "synthesizing" basis vector directions for A. (These are the eigenvectors of AA^T.)
(3) The diagonal values in matrix S are the singular values, which can be thought of as scalar "gain controls" by which each corresponding input is multiplied to give a corresponding output. (These are the square roots of the eigenvalues that correspond with the same columns in U and V.)

The description of these three points are given as follows: Given an SVD of A, as described above, i.e. $A = USV^T$, where U and V are orthnormal matrices, i.e. $U^TU = UU^T = I$ and $V^TV = VV^T = I$. Now, $A^TA = VS^TU^TUSV^T = V(S^TS)V^T \Rightarrow$ the columns of V (right singular vectors) are eigenvectors of A^TA. Again, $AA^T = USV^TVS^TU^T = U(SS^T)U^T \Rightarrow$ the columns of U (left singular vectors) are eigenvectors of AA^T. Consequently, the squares of the non-zero singular values of A are equal to the non-zero eigenvalues of either A^TA or AA^T.

2.3. Automatic thresholding: the Otsu's method

Otsu's method [32] is used to automatically perform the reduction of a gray level image to a binary image via histogram shape-based image thresholding. The algorithm assumes that the image to be thresholded contains two classes of pixels viz. foreground and background followed by the calculation of an optimum threshold by maximizing a discrimimant criterion, i.e., the separability of the resultant classes in gray levels.

Let us assume that the gray level of the given image (I) ranges between $[0, L-1]$, where L is the total number of gray levels of the image. Otsu's method searches for an optimal threshold value T_{opt} in the range such that the objective function $J_{Otsu}(T)$ achieves its maximum. Mathematically,

$$T_{opt} = \arg \max_{0 \le T \le L-1} J_{Otsu}(T) \tag{5}$$

where the objective function is given by

$$J_{Otsu}(T) = \frac{p_1(T)p_2(T)\,(m_1(T) - m_2(T))}{\sigma^2} \tag{6}$$

where $p_1(T) = \sum_{l=0}^{T} h(l) / \sum_{l=0}^{L-1} h(l)$, $m_1(T) = \sum_{l=0}^{T} lh(l) / \sum_{l=0}^{T} h(l)$ denotes the prior probability and the mean of the foreground respectively whereas $p_2(T) = \sum_{l=T+1}^{L-1} h(l) / \sum_{l=0}^{L-1} h(l)$, $m_2(T) = \sum_{l=T+1}^{L-1} lh(l) / \sum_{l=T+1}^{L-1} h(l)$ denotes the prior probability and mean of the background respectively. The $\sigma^2 = \sum_{l=0}^{L-1} (l - m(T))^2\, h(l)$ is the variance of the gray level of the image. $m(t)$ is the mean of total gray levels whereas $\{h(l) : l = 0, 1, \ldots, L-1\}$ is the gray level histogram or distribution of the image. As soon as the optimal threshold is obtained, the binarization of the image I is done as

$$\mathfrak{B}_I(i,j) = \begin{cases} 1, & \text{if } I(i,j) \ge T_{opt} \\ 0, & \text{otherwise.} \end{cases} \tag{7}$$

From Eq. (6), it is clear that maximizing Otsu's objective function equivalently maximizes the between-class separation in the foreground and background while at the same time, minimizes the total variance in both fore- and back-ground classes. It has been shown [32] that the above criterion can achieve its maximum when the distributions of both classes are two-peaked, especially Gaussian with the same class variance. Again from Eq. (6), we can also see that Otsu's criterion pays almost equal attention to both the foreground and background, which is the main benefit of the Otsu's method in thresholding.

3. Redundant fractional wavelet transform (RFrWT)

The continuous fractional wavelet transform (FrWT) [33] of 1D function $f(t) \in L^2(\mathbb{R})$ is written as

$$W^{\alpha}(s,\tau) = \int_{-\infty}^{\infty}\int_{-\infty}^{\infty} K_{\alpha}(t,x)\, f(t)\psi_{s,\tau}(x)dt\ dx \tag{8}$$

where $\psi_{s,\tau}(x)$, α and $K_{\alpha}(t,x)$ are called mother wavelet, transform order and transform kernel respectively associated with FrWT. The mother wavelet is obtained by the dilation (scale) and translation (position) parameters s and τ. Mathematically, the mother wavelet is defined as follows

$$\psi_{s,\tau}(x) = \frac{1}{\sqrt{s}}\psi\left(\frac{x-\tau}{s}\right) \quad \text{satisfying} \int_{-\infty}^{\infty}\psi_{s,\tau}(x)dx = 0, \qquad \int_{-\infty}^{\infty}|\psi_{s,\tau}(x)|^2 dx = 1 \tag{9}$$

and the transform kernel is given as

$$K_{\alpha}(t,x) = C_{\alpha}k_{\alpha}(t,x)e^{-itx\csc\overline{\alpha}} \tag{10}$$

where $k_{\alpha}(t,x) = e^{(i/2)(t^2+x^2)\cot\overline{\alpha}}$ and $C_{\alpha} = e^{i\overline{\alpha}/2}/\sqrt{2\pi i\sin\overline{\alpha}}$. It is clear that if $\overline{\alpha} = \alpha\pi/2$ then $C_{\alpha} = \sqrt{\frac{1-i\cot\alpha}{2\pi}}$. Similarly, if $\sin\overline{\alpha} = 0$ then by a limiting process the kernel reduces to a Dirac delta ($\delta(x \pm t)$). Further, to reconstruct the original signal back from the transformed signal, the inverse fractional wavelet transform is defined as:

$$f(t) = \frac{1}{C_{\psi}}\int_{-\infty}^{\infty}\int_{-\infty}^{\infty}\int_{-\infty}^{\infty} F^{-\alpha}[W^{\alpha}(s,\tau)](x)\ \psi_{s,\tau}(t)\ \frac{ds\,d\tau\ dx}{s^2} \tag{11}$$

where $C_{\psi} = \int_{-\infty}^{\infty}\frac{|\widehat{\psi}(u)|^2}{|u|}du$ with $\widehat{\psi}(u)$, the Fourier Transform of $\psi(t)$. Further, we can rearrange Eq. (8) as

$$W^{\alpha}(s,\tau) = \int_{-\infty}^{\infty} F^{\alpha}[f(t)](x)\ \psi_{s,\tau}(x)\ dx \tag{12}$$

where $F^{\alpha}[f(t)](x)$ is the α-order fractional Fourier transform of the function $f(t)$. From above Eq. (12), it is clear that the FrWT is a realization of the wavelet transform in fractional Fourier domain. Fractional Fourier transform has a unique property of describing the information of spatial and frequency domains, due to the rotation of time-frequency plane over an arbitrary angle whereas wavelet transform has a multiresolution property. A combination of these two domains results in FrWT, that exhibits the multiresolution property and describes the spatial as well as frequency domain information.

In practical problems, most of the signals are discrete–time/discrete signals. A discrete signal is a function (real or complex valued) whose argument runs over the integers, rather than over the real line. Therefore, one cannot apply FrWT directly on the discrete signals. Another problem is that for most functions the FrWT has no analytical solutions and they can be calculated only numerically or by an optical analog computer. Therefore, one needs some fast algorithms to exploit the power and efficiency of the fractional wavelet transform. These issues are resolved by a discretizing continuous fractional wavelet transform, coined as a discrete fractional wavelet transform (DFrWT) [34]. A DFrWT is a sampled fractional wavelet function. Rather than calculating the wavelet coefficients at every point, the DFrWT uses only a subset of positions and scales. This method results in an accurate and more efficient manner of a continuous fractional wavelet transform.

The DFrWT algorithm is easily derived in the same lines as which one can obtain discrete wavelet transform. Therefore, the DFrWT also employs decimators after filtering. As a result, both approximation and detail signals are half as much as the original signal in length after transformation [35]. Like DWT, DFrWT is very efficient from the computational point of view but it has one major drawback, i.e DFrWT is not translation invariant. This drawback has exerted a remarkable influence on several applications such as denoising, estimation, compression etc. It has been shown that the influence could be suppressed by a redundant representation of the signal [36,37] and is obtained easily by omitting the use of decimators from the implementation of DFrWT which results in the redundant fractional wavelet transform (RFrWT) [36].

In this section, we propose a new structure for the RFrWT, based on the second generation wavelets. The second generation wavelets are constructed by the flexible approach of lifting scheme. The idea behind the lifting scheme is to modify the property of a known wavelet and build a new wavelet with some expected properties. This structure can be described as the upsampled predict and update steps without the split stage. The new structure maintains the same performance as other implementations, yet it inherits some benefits through the use of the lifting scheme. These benefits are the integer-to-integer transform, the design simplicity of the inverse transforms and the faster processing speed [37].

To implement RFrWT, the original discrete signal $f[t]$ (we shall use square brackets, as in $f[t]$, for discrete signals and round parentheses, as in $f(t)$, for continuous signals) is first transformed by the fractional Fourier transform followed by the lifting process. The whole lifting scheme is described in the following steps.

1. Perform α-order fractional fourier Transform on the input signal $f[t]$, denoted by $g[t]$.
2. *Split:* Divide the original data into two disjoint subsets. Although any disjoint split is possible we will split the original data set $g[t]$ into $g_e[t] = g[2t]$, the even indexed points and $g_o[t] = g[2t+1]$, the odd indexed points.

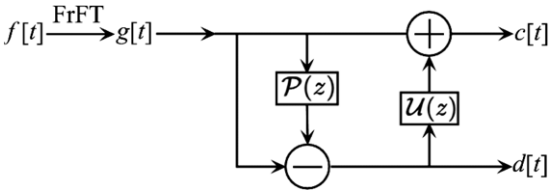

Fig. 2. Implementation of proposed RFrWT.

3. *Predict:* Generate the wavelet coefficients $d[t]$ as the error in predicting $g_o[t]$ from $g_e[t]$ using prediction operator $\mathcal{P}$ i.e.
$$d[t] = g_o[t] - \mathcal{P}(g_e[t]). \tag{13}$$
4. *Update:* Combine $g_e[t]$ and $d[t]$ to obtain scaling coefficients $c[t]$ that represent the coarse approximation to the original signal $g[t]$. This is accomplished by applying an update operator $\mathcal{U}$ to the wavelet coefficients and adding the result to $g_e[t]$ i.e.
$$c[t] = g_e[t] + \mathcal{U}(d[t]). \tag{14}$$

In the above steps, the undecimated 4-point predict and update operators are used [37]. Mathematically, these operators are defined as

$$\mathcal{P}(z) = z^{-1}\mathcal{P}(z^2) = p_1 z^{-3} + p_2 z^{-1} + p_3 z^1 + p_4 z^3 \tag{15}$$
$$\mathcal{U}(z) = z^{-1}\mathcal{U}(z^2) = u_1 z^{-3} + u_2 z^{-1} + u_3 z^1 + u_4 z^3. \tag{16}$$

From Eqs. (15) and (16), it is clear that the time-varying decimators have been removed and the shift-invariance is ensured in the transform. The complete implementation of the RFrWT is depicted in the Fig. 2.

In Fig. 3, the comparison between redundant wavelet transform (RWT) and the proposed RFrWT is depicted using an absolute normalized Sinc signal. Mathematically, the absolute normalized Sinc signal is expressed as

$$f(x) = |\mathrm{Sinc}(x)| = \left|\frac{\sin \pi x}{\pi x}\right|. \tag{17}$$

In this experiment, the 5-level of decomposition is considered and 0.5 is used as transform order for RFrWT. First, we discuss redundant wavelet transform. In RWT, the approximate part is the sub-sampled version of the signal and hence, it follows the shape of the signal. The detail part, on the other hand, actually provides the changes in signal values in subsequent samples. This implies that the detailed part describes the derivatives of the signal itself. This can be explained using the Fig. 3. The peaks or extremas of the signal produce zero derivative. Thus, the detail part is zero at these instances. Again, when the signal rapidly decreases or increases, the changes in successive samples are larger producing maximas or minimas in the derivative. Thus, the detail part contains extremas at the sudden changes of the signal. On the contrary, RFrWT also follows the same phenomena but it will give uniform randomness to the detailed parts. Fig. 3 clearly shows that the detailed parts of RWT are smooth when compared to RFrWT's detailed parts.

Till now, the behavior of RFrWT has not been discussed with varying transform orders. In this experiment, the 1-level of decomposition is used in order to get better visualization. Fig. 4 gives the assessment of RFrWT using different transform orders. RFrWT will give randomness to coefficients that lie on either local maxima or local minima whereas the randomness is much less (negligible) in the case of global maxima or minima. Further, if the value of α is varied, the coefficients lying in local maxima or local minima are going to become smooth (constant) and only global maxima and minima exist as α approaches to 1.

From the above discussion, it is clear that different transform orders produce different randomness in the transformed signal which will be maximum whenever transform order reaches to 1. Therefore, when an application needs the randomness as its key factor, RFrWT must provide better results. In order to support our claim, we have also done the randomness analysis on the RWT and RFrWT.

The entropy of the transform coefficient distribution is a common measure of the efficiency of a signal transform. The entropy of the coefficient distribution appears as a measure of the degree of order/disorder (randomness) that the signal possesses. In general, the smaller values of entropy exhibit the less randomness in the coefficients. In the experiments, the entropies of the coefficient distributions of several well known test signals are compared to assess the level of compaction afforded by the new transform over RWT. Let us collectively denote the scaling and wavelet coefficients by $\{C_i\}$ then the entropy is defined as

$$H(C) = \sum_i |C_i|^2 \log_2 |C_i|^2 \tag{18}$$

assuming the normalization $\sum_i |C_i|^2 = 1$. Table 1 compares the entropies of the RWT and RFrWT coefficients distribution for five commonly used signals namely, rectangular, Sine, Cosine, normalized Sinc and absolute normalized Sinc signals

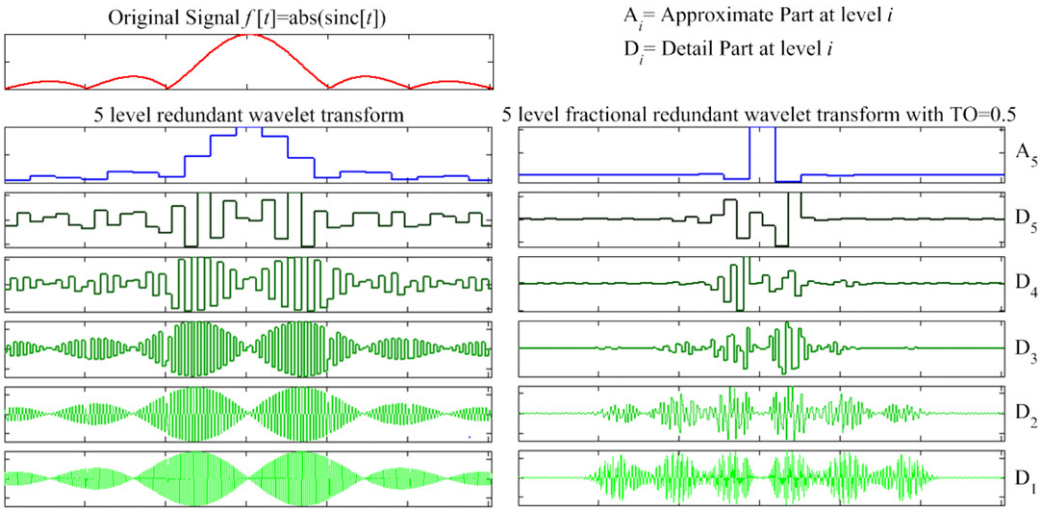

Fig. 3. Comparison between RWT and RFrWT considering five levels of decomposition and sinc signal.

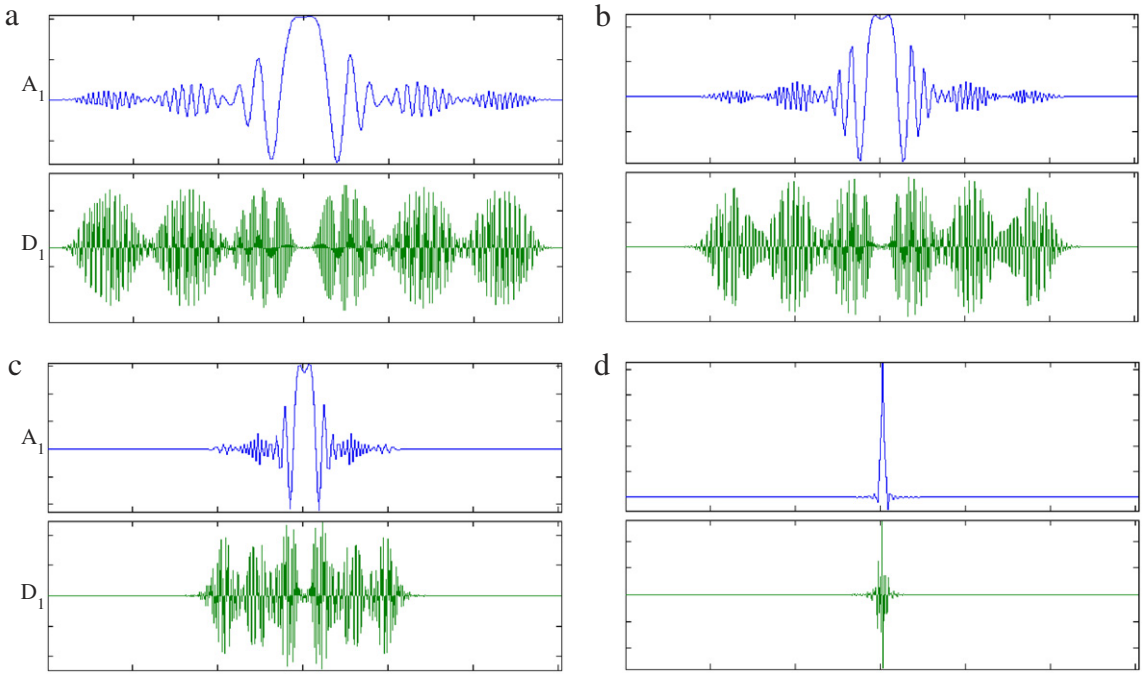

Fig. 4. Visual assessment of RFrWT approximate and detail subbands associated with different transform orders.

respectively. These signals are decomposed by 5 level of RWT and RFrWT followed by the entropy calculation using Eq. (18). From the table, it is clear that the entropy increases with RFrWT compared to RWT. The entropy for RWT is much less (close to zero) which says that there is no randomness in the coefficients distribution whereas RFrWT gives randomness with respect to RWT but the randomness depends on the transform order and reaches maximum when $\alpha = 1$. This ability of RFrWT proves its superiority over RWT in the sense that for every different α, different randomness is obtained in the coefficients.

4. Proposed watermarking technique

In this section, we discuss some motivating factors in the design of our approach to watermarking. The proposed algorithm uses two watermarks out of which one is a gray scale logo whereas the second is a binary image. The initial watermarks used for embedding are equal in size when compared with the host image. Without loss of generality, assume that G represents the host image of size $M \times N$ whereas W_1 and W_2 represent the initial watermarks of size $M \times N$.

Table 1
Entropy comparison between RWT and RFrWT.

Transform	Entropy in the signal				
	Rectangular	Sine	Cosine	Sinc	Absolute Sinc
RWT	0.0237	0.0178	0.0128	0.0249	0.0704
RFrWT	2.1190	2.2238	2.8909	2.2575	2.9293

4.1. Reversible extension transform (RET)

The Reversible Extension Transform (RET) is a reversible transform which maps an image into another image such that the size of obtained image is greater then of original. Since the size of image is increased we therefore coined it a reversible extension transform. Mathematically, the RET G_{RET} (say) of image G is given as

$$\begin{aligned} G_{RET}(2i-1, 2j-1) &= G(i, j) \\ G_{RET}(2i-1, 2j) &= G(i, j) \\ G_{RET}(2i, 2j-1) &= G(i, j) \\ G_{RET}(2i, 2j) &= G(i, j). \end{aligned} \tag{19}$$

In order to get the original image back from the extended image, the inverse reversible extension transform is given as

$$G(i, j) = \frac{1}{4} \sum_{m=0}^{1} \sum_{n=0}^{1} G_{RET}(2i-m, 2j-n). \tag{20}$$

If Eq. (19) is observed then it is clear that the size of extended image G_{RET} is just the double of original image G. In other words, the size of G_{RET} is $2M \times 2N$ whereas Eq. (20) maps the extended image to its original size $M \times N$.

4.2. Watermark embedding algorithm

The embedding algorithm to embed the gray scale logo and binary image is formulated as follows:

1. The size of host image is scaled-up via reversible extension transform, denoted by $G_{RET} = F$.
2. Perform L-level (α_x, α_y)-order redundant fractional wavelet transform on F, which is denoted by f_l^{θ}, where $\theta \in \{A, H, V, D\}$ and $l \in [1, L]$.
3. *Embedding Gray Scale Logo*: The gray scale logo (W_1) is embedded in the low frequency sub-band at the finest level i.e. f_L^A and the process is formulated as follows:
   (a) Perform SVD on both f_L^A and W_1
   $$f_L^A = U_{f_L^A} S_{f_L^A} V_{f_L^A}^T, \qquad W_1 = U_{W_1} S_{W_1} V_{W_1}^T. \tag{21}$$
   (b) Modify the middle singular values of f_L^A with the help of watermark singular values as
   $$S_{f_L^A}^*(i+p) = S_{f_L^A}(i+p) + \beta S_{W_1}(i) \tag{22}$$
   where β gives the watermark strength, $i = 1, 2, \ldots, \min(M, N)$ and p is the factor for choosing middle singular values. For example, if the value of p is 63 then the watermark singular values are embedded among 64 to $63 + \min(M, N)$ singular values of f_L^A sub-band.
   (c) Perform inverse SVD to construct modified sub-band
   $$f_L^{A,\,new} = U_{f_L^A} S_{f_L^A}^* V_{f_L^A}^T. \tag{23}$$
4. Perform L-level (α_x, α_y)-order inverse redundant fractional wavelet transform to get the watermarked extended image, denoted by F^{new}.
5. Perform inverse reversible extension transform on the watermarked extended image F^{new} to get the watermarked image denoted by $G^{new} = Gw$.
6. *Verification Step Casting/Embedding Binary Image*: The binary image (W_2) is embedded as follows:
   (a) Shuffle the watermarked image using Arnold cat map p times which is denoted by G_{suf}^{new}.
   (b) Find a binary image $\mathfrak{B}_{G_{suf}^{new}}$ corresponding to G_{suf}^{new} using automatic thresholding.
   (c) Produce the extraction key using bit-wise exclusive-OR operation as:
   $$K = XOR(\mathfrak{B}_{G_{suf}^{new}}, W_2). \tag{24}$$
   After the extraction key K is constructed, the embedding process is completed. Obviously, G^{new} also remains unchanged during this embedding.

4.3. Watermark extraction algorithm

The objective of the watermark extraction algorithm is to obtain the estimate of the original watermark. For binary watermark extraction, only key K is required whereas for gray scale logo extraction, host G and watermarked image Gw, p, V_{W_1} and U_{W_1} are required. Hence, the binary watermark extraction is blind and gray-scale watermark extraction is non-blind. The extraction process is formulated as follows:

1. Shuffle the watermarked image using Arnold cat map p times which is denoted by Gw_{suf}.
2. Find a binary image $\mathfrak{B}_{G_{suf}}$ corresponding to Gw_{suf} using automatic thresholding.
3. *Verification step: Extracting binary image*: The binary watermark is extracted using bit-wise exclusive-OR operation as:
$$W_2^{ext} = XOR(\mathfrak{B}_{G_{suf}}, K). \tag{25}$$
4. *Extracting gray scale logo*: This extraction is performed if and only if the similarity between extracted (from previous step) and original binary watermark is greater than the prescribed threshold. The gray-scale extraction process is described as follows:
   (a) The size of watermarked image is scaled-up via reversible extension transform, denoted by $Gw_{RET} = Fw$.
   (b) Perform L-level (α_x, α_y)-order redundant fractional wavelet transform on Fw, which is denoted by fw_l^{θ}, where $\theta \in \{A, H, V, D\}$ and $l \in [1, L]$.
   (c) Select the low frequency sub-band at the finest level i.e. fw_L^A to extract the gray scale logo.
   (d) Perform SVD on fw_L^A
   $$fw_L^A = U_{fw_L^A} S_{fw_L^A} V_{fw_L^A}^T. \tag{26}$$
   (e) Extract the singular values of gray scale logo as
   $$S_{W_1}^{ext}(i) = \frac{S_{fw_L^A}(i+p) - S_{f_L^A}(i+p)}{\beta}. \tag{27}$$
   (f) Perform inverse SVD to construct the extracted gray-scale logo.
   $$W_1^{ext} = U_{W_1} S_{W_1}^{ext} V_{W_1}^T. \tag{28}$$

5. Results and discussions

5.1. Experimental setup

The robustness of the proposed watermarking algorithm is demonstrated using the MATLAB platform and different standard test images namely Mandril, Cameraman, Lena and Lady of size 256×256 are used as the host images. For gray scale logo watermarks, Peacock, ACM logo, University of Windsor logo and IEEE logo of size 256×256 is used whereas Dollar and full form of ACM, University of Windsor, and IEEE are used as the binary watermarks. The watermarked image quality is measured using PSNR and SSIM. Mathematically, PSNR and SSIM are defined as follows.

1. Peak Signal to Noise Ratio (PSNR): The PSNR indicates the similarity between two images. The higher the value of PSNR, the greater the similarity in the images. Mathematically, PSNR is defined as
$$PSNR(f, g) = 10 \log_{10} \frac{255^2}{\frac{1}{MN} \sum_{i=1}^{M} \sum_{j=1}^{N} [f_{i,j} - g_{i,j}]^2} \tag{29}$$
   where MN is the total number of pixels in the image, $f_{i,j}$ and $g_{i,j}$ are the values of the ijth pixel in the original and encrypted image.
2. Structural Similarity Index Measure (SSIM): The SSIM indicates the similarity in the structure of the two images. The value of SSIM lies between $[-1,\ 1]$ and the value closer to 1, the greater similarity in the images. Mathematically, SSIM is defined as
$$SSIM(f, g) = \frac{(2\mu_f \mu_g + C_1)(2\sigma_{fg} + C_2)}{(\mu_f^2 + \mu_g^2 + C_1)(\sigma_f^2 + \sigma_g^2 + C_2)} \tag{30}$$
   where μ_f, μ_g, σ_f, σ_g and σ_{fg} are the mean of f and g, variance f and g and the covariance of f and g respectively. The constants $C_1,\ C_2$ are used to stabilize the division with a weak denominator.

The PSNR and SSIM values for the watermarked images are given in the Table 2 whereas the original host, watermarked, original watermark and extracted watermark images are shown in Fig. 5. From the figure and table, it is clear that there is no perceptual degradation between the original and the watermarked images according to human perception. The value of watermark strength (β) is calculated by attempting several experiments on the host image considering human visual system. For this purpose, watermark images are prepared with the different values of β and some human observers are asked to view a series of watermarked images and rate them. The value of β is taken to be optimal for which most of observers fail to distinguish the original and watermarked image.

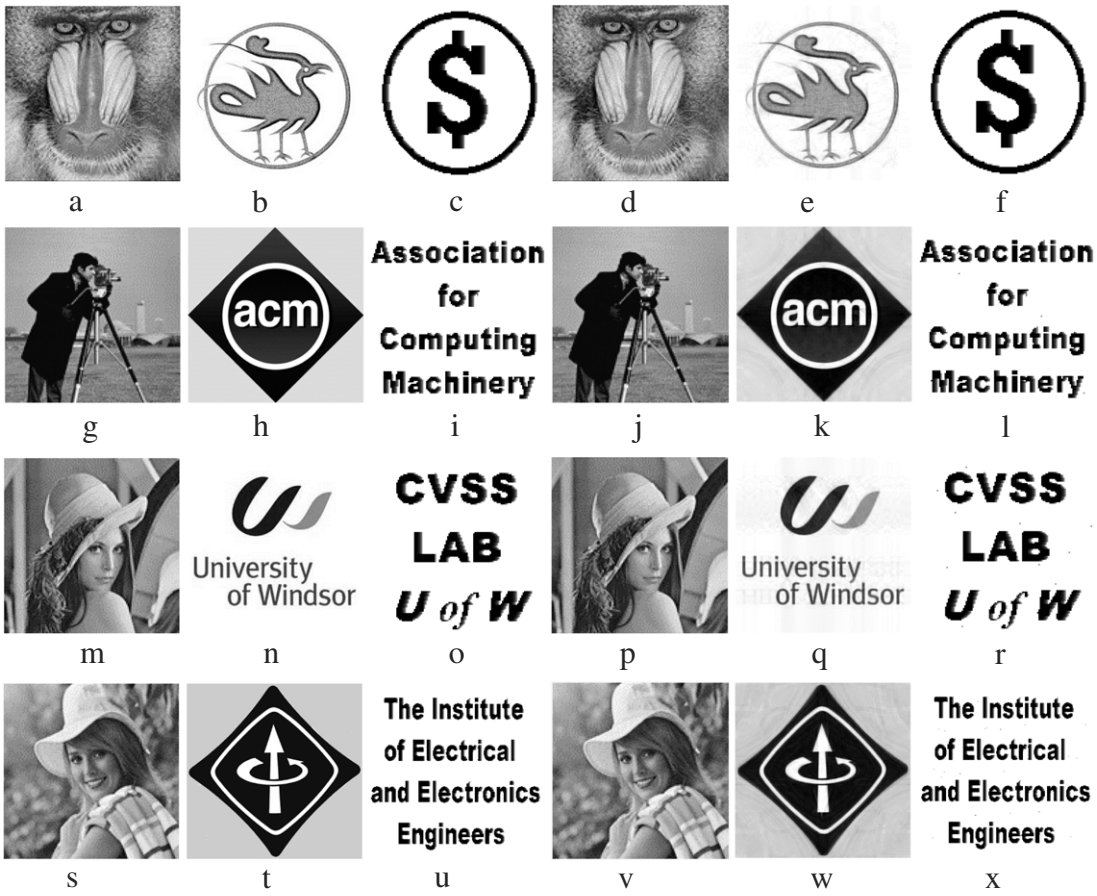

Fig. 5. (a, g, m, s) Original host (b, h, n, t) Original gray-scale watermark (c, i, o, u) Original binary watermark (d, j, p, v) Watermarked (e, k, q, w) Extracted gray-scale watermark (f, l, r, x) Extracted binary watermark images.

Table 2
Imperceptibility of the proposed watermarking technique.

Metric	Images			
	Mandrill	Cameraman	Lena	Lady
PSNR	38.5681	40.7458	39.9853	39.7118
SSIM	0.9983	0.9999	0.9991	0.9995

To verify the presence of the watermark, the correlation coefficient between the original and the extracted watermark is given by

$$\rho(w, \bar{w}) = \frac{\sum_{i=1}^{M_1}\sum_{i=1}^{N_1} (w(i) - \mu_w)\,(\overline{w}(i) - \overline{\mu}_w)}{\sqrt{\sum_{i=1}^{M_1}\sum_{i=1}^{N_1} (w(i) - \mu_w)^2}\sqrt{\sum_{i=1}^{M_1}\sum_{i=1}^{N_1} (\overline{w}(i) - \overline{\mu}_w)^2}} \tag{31}$$

where w, $\overline{w}$, μ_w and $\overline{\mu}_w$ are the original, extracted, mean of original and extracted watermarks. ρ is the number that lies between $[-1, 1]$. If the value of ρ is equal to 1 then the extracted singular values are just equal to the original one, if it is -1 then the constructed watermark looks like a negative thin film. In order to evaluate the similarity between binary watermarks, the threshold is set to be 0.6.

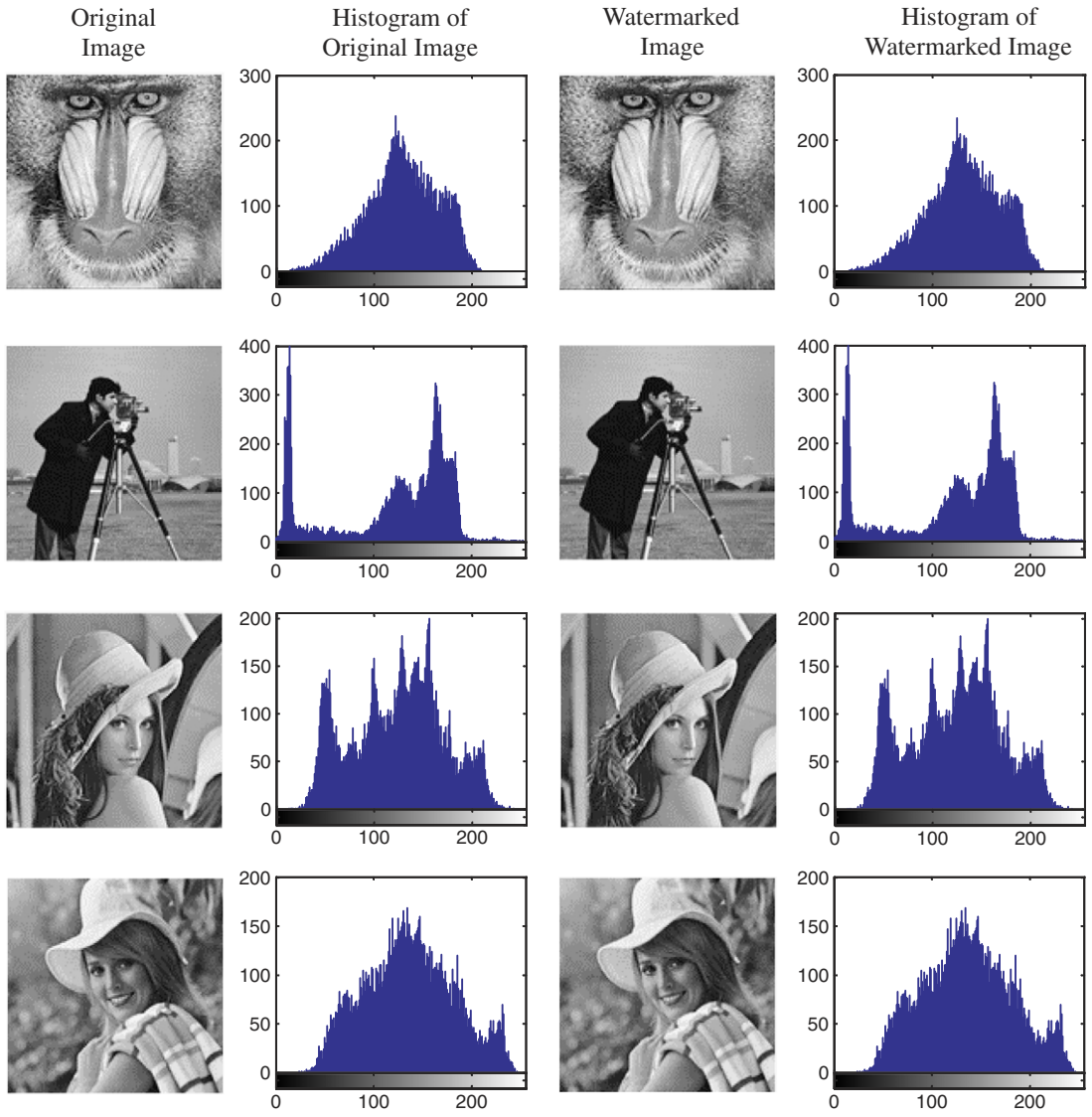

Fig. 6. Imperceptibility of the proposed technique via histogram.

5.2. Imperceptibility of the proposed technique: histogram analysis

Imperceptibility or transparency relates to the properties of the human visual system. In general, if the original and the watermarked images are (close to) being perceptually indistinguishable, the watermarking technique is said to be imperceptible. In other words, a good watermarking technique causes no artifacts or quality loss in the images. In order to judge the imperceptibility, objective and subjective processes are used. In the objective process, the imperceptibility is carried out by the use of quality metrics (the imperceptibility of proposed technique by objective process is provided in the Section 5.1 considering PSNR and SSIM quality metrics). On the contrary, the subjective process takes advantage of the tonal distribution comparison between original and watermarked images [38]. The best way to obtain tonal distribution of an image is the histogram. Therefore, we compare the histogram of the original and watermarked images to show the imperceptibility.

A histogram is basically a graphical representation of the tonal distribution in the image. In other words, a histogram is a graph which shows the size of the area of the image that is captured for each tonal variation that the camera is capable of recording. By looking at the histogram for a specific image, we will be able to judge the entire tonal distribution at a glance. It tells us how much detail is at the light end of the spectrum and how much at the dark [39]. In Fig. 6, the histogram analysis for all the experimental images are shown. It is clear from the figure that the overall shape of the histogram is similar i.e. the tonal distribution of the original and watermarked images are similar which further proves the imperceptibility of the proposed technique.

Fig. 7. Watermarked images after (a) Gaussian blurring (7 × 7) (b) Gaussian noise addition (50%) (c) Salt & pepper noise addition (50%) (d) JPEG compression (80:1) (e) SPIHT compression (0.1 bpp) (f) Resizing (256 → 64 → 256) (g) Rotation (30°) (h) Wrapping (i) Histogram equalization (j) Sharpen (increased by 80%) (k) Contrast adjustment (decreased by 80%).

5.3. Attack analysis

We investigate the robustness of the algorithm by considering Gaussian blurring, Gaussian and Salt & Pepper noise addition, JPEG & SPIHT compression, Resize, Rotation, Histogram Equalization, Wrapping, Sharpen and Contrast Adjustment attacks on the watermark image. After these attacks on the watermarked image, extracted watermarks are compared with the original one. Further, the visual results are shown for the Cameraman image because it has maximum PSNR and SSIM values whereas quantitative results are shown for all the experimental images. In Fig. 7, attacked watermarked Cameraman images are shown after a variety of attacks. The detailed description of these attacks is as follows.

The most common manipulation in a digital image is blurring. One of the widely used blurrings is Gaussian blurring which can be found in graphics software, typically to reduce image noise and increase smoothness. The extracted watermarks, after blurring a watermarked image considering a 7 × 7 window, are shown in the Fig. 8(I). To verify the robustness of the watermarking scheme, another measure is noise addition. In our experiments, P% additive Gaussian and Salt & Pepper noise are added in the watermarked image. In Fig. 8(II) and (III), extracted watermarks from 50% Gaussian and Salt & Pepper noise attacked watermarked images are shown. Storage and transmission of digital data is the most common operation, and for this purpose a lossy coding operation is often performed on the data to reduce the memory and increase efficiency. Hence, we have also tested our algorithm for JPEG & SPIHT compression and the results are shown in Fig. 8(IV)–(V). For JPEG compression, the watermarked image is compressed up to 80:1 whereas for SPIHT compression the image is compressed up to 0.1 bpp. The proposed algorithm has also been tested for resizing and rotation attacks. For resizing, the size of the image is reduced to 64 × 64 and then again carried back to the original size 256 × 256, see Fig. 8(VI). For rotation attack, the watermarked image is rotated with an angle 30° and the concerned result is depicted in Fig. 8(VII). Results for wrapping and histogram equalization attacks are shown in Fig. 8 (VIII)–(IX) respectively. Wrapping is the process of giving a 3D effect to an object by folding a selection around a shape. Fig. 8(VIII) shows the extracted watermarks when an object is wrapped around a spherical shape. We have also tested our proposed watermarking algorithm for histogram equalization, sharpen and contrast adjustment attacks. For the sharpen attack, the sharpness of the watermarked image is increased by a factor of 80 and then watermarks are extracted, see Fig. 8(X), whereas for contrast adjustment, the contrast of the watermarked image is decreased by 80%, see Fig. 8(XI). The corresponding correlation coefficient values for all extracted watermark images

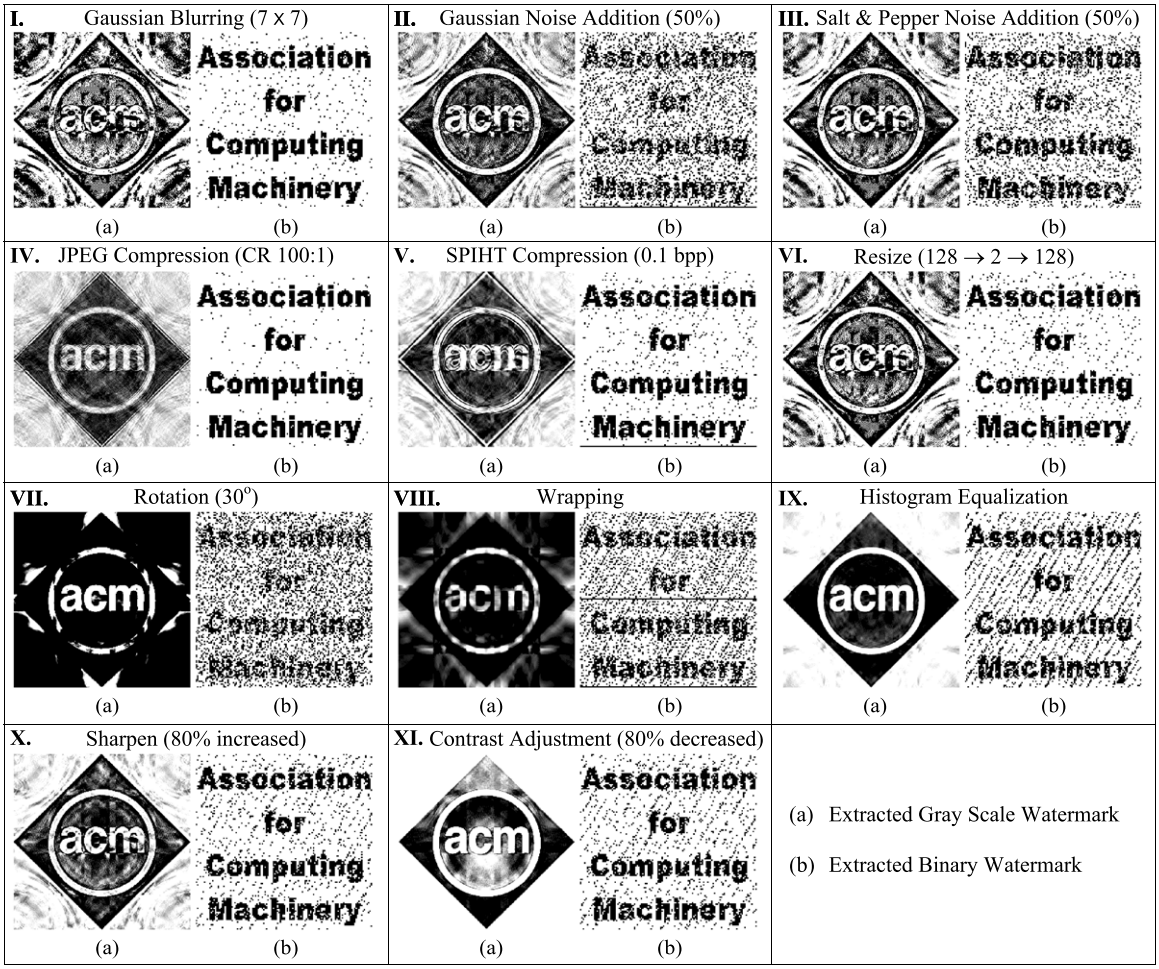

Fig. 8. Extracted watermarks from cameraman image after attacks.

Table 3
Correlation coefficients for the extracted watermarks.

Attacks	ρ							
Watermarks	Mandrill		Cameraman		Lena		Lady	
	Binary	Gray-scale	Binary	Gray-scale	Binary	Gray-scale	Binary	Gray-scale
No attack	0.9998	0.9993	0.9996	0.9991	0.9999	0.9992	0.9999	1
Gaussian blurring	0.9809	0.4614	0.9766	0.4608	0.9863	0.5140	0.9833	0.5258
Gaussian noise addition	0.8631	0.5266	0.8599	0.5279	0.8658	0.5311	0.8689	0.5383
Salt & pepper noise addition	0.9152	0.6555	0.9020	0.6583	0.9078	0.6591	0.9133	0.6656
JPEG compression	0.9939	0.9917	0.9922	0.9908	0.9979	0.9834	0.9961	0.9919
SPIHT compression	0.9842	0.8596	0.9763	0.8530	0.9755	0.8551	0.9830	0.8528
Resizing	0.9728	0.6663	0.9759	0.6613	0.9768	0.6686	0.9797	0.6541
Rotation	0.7535	0.6576	0.7500	0.6567	0.7592	0.6606	0.7582	0.6591
Wrapping	0.8757	0.6631	0.8785	0.6628	0.8701	0.6690	0.8859	0.6691
Histogram equalization	0.9296	0.9952	0.9247	0.9871	0.9277	0.9910	0.9261	0.9921
Sharpen	0.9571	0.7835	0.9562	0.7856	0.9542	0.7917	0.9597	0.7992
Contrast adjustment	0.9569	0.9909	0.9509	0.9937	0.9537	0.9941	0.9593	0.9956

are given in Table 3. Table 3 shows the improved performance in terms of imperceptibility and robustness against different kinds of attacks.

5.4. Security analysis

Security is the main thrust in the watermarking techniques. In general, a highly key sensitive watermarking technique protects the data against various attacks because slight change in the keys never gives the perfect extraction which further

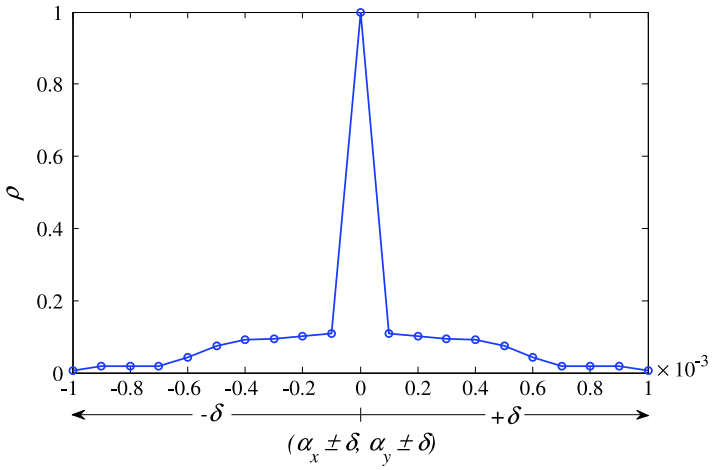

Fig. 9. Security analysis of the proposed watermarking technique.

increases the security. Therefore, keys play the vital role to enhance the security. Hence, the key sensitivity of the proposed technique is validated. For this purpose, it is assumed that an intruder knows the complete embedding and extraction structure but not the used key. In the proposed technique, two keys (α_x and α_y) are used. These keys are used as the transform order for RFrWT. The sensitivity is checked in three cases (1) when α_x is slightly changed (2) when α_y is slightly changed (3) when both α_x and α_y both are slightly changed. The slight change is made in such a way that the original and modified keys are approximately same. In the experiments, the values of α_x and α_x are 0.2551 and 0.9593 respectively. In this experiment, the keys are modified as $\alpha_i \pm \delta : i = x, y$ where $\delta \in [0, 0.001]$. Fig. 9 shows the quality of extracted gray-scale watermark with respect to varying keys α_x and α_y. It is clear from the figure that the similarity between the extracted and original watermarks degrades as the keys are changed slightly. Therefore, the proposed technique is highly sensitive to the keys α_x and α_y. Hence, without knowing the correct values of the key none can extract the watermarks perfectly even he/she knows the complete technique structure.

6. Conclusions

In this paper, a robust watermarking scheme is presented based on redundant fractional wavelet transform, reversible extension transform and singular value decomposition (SVD) in which the two watermarks are embedded. These two watermarks are visually meaningful gray scale and binary image/logo respectively instead of a noise type Gaussian sequence. The key factor of the proposed scheme is the use of redundant fractional wavelet transform and the factor for choosing middle singular values (p) gives more complexity to the extraction process because without knowing these values no attacker can extract the data correctly. Further, the verification step, done via automatic thresholding, has enhanced the security by giving authentication to the possibly attacked watermarked image. For extraction, the reliable extraction scheme is constructed for the binary and also for gray-scale watermarks. The feasibility and the robustness of the proposed method are carried out by a variety of attacks. Further, a new transform namely redundant fractional wavelet transform is also proposed in the present work. The new transform can be used in all those applications where randomness is the key factor like information security.

Acknowledgments

The work is supported in part by the Canada Research Chair program, and the Natural Sciences and Engineering Research Council of Canada.

References

[1] R.G.V. Schyndel, A.Z. Tirkel, C.F. Osbrone, A digital watermark, in: Proc. of IEEE Int. Conf. on Image processing, vol. 2, 1994, pp. 86–90.
[2] I.-S. Lee, W.-H. Tsai, Data hiding in grayscale images by dynamic programming based on a human visual model, Pattern Recognition 42 (7) (2009) 1604–1611.
[3] V. Martin, M. Chabert, B. Lacaze, An interpolation-based watermarking scheme, Signal Processing 88 (3) (2008) 539–557.
[4] T.-Y. Lee, S.D. Lin, Dual watermark for image tamper detection and recovery, Pattern Recognition 41 (11) (2008) 3497–3506.
[5] I.J. Cox, J. Killian, F.T. Leighton, T. Shamoon, Secure spread spectrum watermarking for multimedia, IEEE Transactions on Image Processing 6 (12) (1997) 1673–1687.
[6] M. Barni, F. Bartiloni, V. Cappellini, A. Piva, A DCT domain system for robust image watermarking, Signal Processing 66 (3) (1998) 357–372.
[7] I. Djurovic, S. Stankovic, I. Pitas, Digital watermarking in the fractional fourier transformation domain, Journal of Network and Computer Applications 24 (4) (2001) 167–173.

[8] Z. Feng, M. Xiaomin, Y. Shouyi, Multiple-chirp typed blind watermarking algorithm based on fractional Fourier transform, in: Proc. of Int. Sym. on Intelligent Signal Processing and Communication Systems, 2005, pp. 141–144.
[9] M. Barni, F. Bartolini, A. Piva, Improved wavelet based watermarking through pixel wise masking, IEEE Transactions on Image Processing 10 (2001) 783–791.
[10] D. Kundur, D. Hatzinakos, Towards robust logo watermarking using multiresolution image fusion, IEEE Transactions on Multimedia 6 (2004) 185–197.
[11] S.H. Wang, Y.P. Lin, Wavelet tree quantization for copyright protection watermarking, IEEE Transactions on Image Processing 13 (2) (2004) 154–165.
[12] X.D. Zhang, J. Feng, K.T. Lo, Image watermarking using tree-based spatial-frequency feature of wavelet transform, Journal of Visual Communication and Image Representation 14 (2003) 474–491.
[13] S.M.M. Rahman, M.O. Ahmad, M.N.S. Swamy, A new statistical detector for DWT-based additive image watermarking using the Gauss–Hermite expansion, IEEE Transactions on Image Processing 18 (8) (2009) 1782–1796.
[14] T.-C. Lin, C.-M. Lin, Wavelet-based copyright-protection scheme for digital images based on local features, Information Science 179 (19) (2009) 3349–3358.
[15] C.-H. Chou, K.-C. Liu, A perceptually tuned watermarking scheme for color images, IEEE Transactions on Image Processing 19 (11) (2010) 2966–2982.
[16] J.L. Vehel, A. Manoury, Wavelet packet based digital watermarking, in: Proc. of Int. Conf. on Pattern Recognition, ICPR-2000, vol. 3, 2000, pp. 413–416.
[17] G. Bhatnagar, B. Raman, Robust reference-watermarking scheme using wavelet packet transform and bidiagonal-singular value decomposition, International Journal of Image and Graphics 9 (3) (2009) 449–477.
[18] R. Liu, T. Tan, An SVD-based watermarking scheme for protecting rightful ownership, IEEE Transactions on Multimedia 4 (1) (2002) 121–128.
[19] D.V.S. Chandra, Digital image watermarking using singular value decomposition, in: Proc. of IEEE Midwest Symposium on Circuits and Systems, 2002, pp. 264–267.
[20] E. Ganic, A.M. Eskicioglu, Robust embedding of visual watermarks using DWT-SVD, Journal of Electronic Imaging (2005).
[21] A. Sverldov, S. Dexter, A.M. Eskicioglu, Robust DCT-SVD domain image watermarking for copyright protection: embedding data in all frequencies, in: European Signal Processing Conference, 2005.
[22] Q. Li, C. Yuan, Y.Z. Zong, Adaptive DWT-SVD domain image watermarking using human visual model, in: Proc. of Int. Conf. on Advanced Communication Technology, ICACT-2007, 2007, pp. 1947–1951.
[23] G. Bhatnagar, B. Raman, A new robust reference watermarking scheme based on DWT-SVD, Computer Standards & Interfaces 31 (5) (2009) 1002–1013.
[24] C.C. Chang, P. Tsai, C.C. Lin, SVD-based digital image watermarking scheme, Pattern Recognition Letters 26 (2005) 1577–1586.
[25] G. Bhatnagar, B. Raman, Q.M.J. Wu, Robust watermarking using fractional wavelet packet domain, IET Image Processing 6 (2012) 386–397.
[26] G. Bhatnagar, Q.M.J. Wu, B. Raman, A new robust adjustable logo watermarking scheme, Computer & Security 31 (2012) 40–58.
[27] G. Bhatnagar, B. Raman, A new SVD based watermarking framework in fractional fourier domain, in: Proc. of Int. Conf. on Contemporary Computing, vol. 1, 2010, pp. 107–118.
[28] M. Pollicott, M. Yuri, Dynamical systems and ergodic theory, in: London Mathematical Society Student Text Series, Cambridge, 1998.
[29] E. Beltrami, Sulle funzioni bilineari (On Bilinear Functions), Giornale di Matematiche ad Uso degli Studenti Delle Universita, vol. 11, 1873, pp. 98–106. An English translation by D. Boley is available in Tech. Report 90-37, Dept. of Computer Science, Univ. of Minnesota, Minneapolis, 1990.
[30] C. Jordan, Memoire sur les formes bilineaires (Memoir on Bilinear Forms), Journal de Mathematiques Pures et Appliquees, Deuxieme Serie 19 (1874) 35–54.
[31] C. Eckart, G. Young, The approximation of one matrix by another of lower rank, Psychometrika 1 (1936) 211–218.
[32] N. Otsu, A threshold selection method from gray-level histograms, IEEE Transactions on Systems, Man and Cybernetics 9 (1) (1979) 62–66.
[33] V. Huang, B. Suter, The fractional wave packet transform, Multidimensional Systems and Signal Processing 9 (4) (1998) 399–402. Springer.
[34] Linfei Chen, Daomu Zhao, Optical image encryption based on fractional wavelet transform, Optical Communications 254 (4-6) (2005) 361–367.
[35] S.G. Mallat, A theory for multiresolution signal decomposition: the wavelet representation, IEEE Transactions on Pattern Analysis and Machine Intelligence 11 (1989) 674–693.
[36] A.R. Calderbank, Ingrid Daubechies, Wim Sweldens, Boon-Lock Yeo, Wavelet transforms that map integers to integers, Applied and Computational Harmonic Analysis 5 (3) (1998) 332–369.
[37] C.S. Lee, C.K. Lee, K.Y. Yoo, New lifting based structure for undecimated wavelet transform, Electronics Letters 36 (2000) 1894–1895.
[38] G. Bhatnagar, B. Raman, Distributed multiresolution discrete fourier transform and its application to watermarking, International Journal of Wavelet, Multiresolution and Information Processing 8 (2) (2010) 225–241.
[39] A.C. Bovik, Basic gray-level image processing, in: A.C. Bovik (Ed.), The Handbook of Image and Video Processing, second ed., Academic Press, New York, 2005, pp. 21–37.